PAPER

Check for updates

Acceptor–donor–acceptor (A–D–A) derivatives based on dibenzochrysene

Félix Gagnon, [a] Chloé Dindault, [b] Eve Paradis,[a] Guillaume Wantz [b] and Jean-François Morin *[a]

Novel non-fullerene acceptors (NFAs) derived from vat orange 1 in an A–D–A architecture were synthesized using diphenylamine moieties as solubilizing groups. The optoelectronic properties of these novel NFAs were characterized using UV-visible spectroscopy and electrochemistry, and their thermal properties were assessed by thermogravimetric analysis (TGA) and differential scanning calorimetry (DSC). The NFAs were tested in organic solar cells (OSC). Two architectures (direct and inverted) of OSC were investigated using poly(3-hexylthiophene) (P3HT) for the bulk heterojunction (BHJ) blends. Power conversion efficiency (PCE) values of up to 0.4% have been obtained with P3HT in an inverted architecture. Computational chemistry calculations were carried out using three methods—B3LYP, ωB97xD, and HF/PBE0—to evaluate the preferred conjugation axis in dibenzo[*b,def*]chrysene-based systems, comparing the 2,9-axis (this work) with the previously proposed 7,14-axis, to guide the design of future A–D–A architectures.

Introduction

In the last decade, vat dyes have attracted a lot of interest as building blocks for the preparation of organic semiconductors due to their accessibility, low cost and ease of modifications. Vat dyes possess extended π-conjugated system and absorb light in the visible range, which makes them useful for optoelectronic applications. Among other dyes, 4,10-dibromoanthanthrone (VO3, also called vat orange 3, pigment red 168, C.I. 59300 and vat brilliant orange 3RK)[1] is particularly interesting as it possesses synthetic handles (ketones and bromines) that allows functionalization and, consequently, modulation of its optoelectronic properties. Vat orange 3 has been used for the synthesis of π-conjugated polymers,[2,3] polyradicaloid materials,[4] dispersing agents for carbon nanomaterials[5] and biological sensing probes.[6] Other derivatives have been developed for organic solar cells (OSCs)[7,8] and organic field-effect transistor (OFET) applications.[2,9] Although interesting, vat orange 3 showed some limitations for the preparation of low band gap molecules and polymers due to the presence of a hydrogen atom in the *peri* position relative to the bromine, inducing a large dihedral angle between the anthanthrene core and the adjacent units attached at the 4 and 10 positions (Fig. 1b).[10]

To overcome this issue, another vat dye, 2,9-dibromo-dibenzo[*b,def*]chrysene-7,14-dione (VO1, also called vat orange 1, C.I. 59105 and vat golden yellow RK), which is another hexacyclic unsaturated core that possesses the same chemical handles as vat orange 3, has been explored.[11,12] Unlike vat orange 3, the bromine atoms are located on the scaffold of vat orange 1 so that there is much less induced steric hindrance when other π-conjugated units are attached at these positions (Fig. 1c). The dibenzo[*b,def*]chrysene-7,14-dione motif has been studied for their crystal structures[13–15] and used as p-type material in OSCs[16,17] and in OFETs.[18–20]

Recently, we reported the use of vat orange 1 as a building block for the preparation of conjugated polymers for OFET and OSC applications.[12] By incorporating various comonomers, polymers with band gap values as low as 1.58 eV have been

[a] Département de Chimie and Centre de Recherche sur les Matériaux Avancés (CERMA), Université Laval, Pavillon A.-Vachon. 1045 Ave de la Médecine, Québec, G1V 0A6, Canada. E-mail: jean-francois.morin@chm.ulaval.ca

[b] Univ. Bordeaux, CNRS, Bordeaux INP, IMS, UMR 5218, F-33400 Talence, France
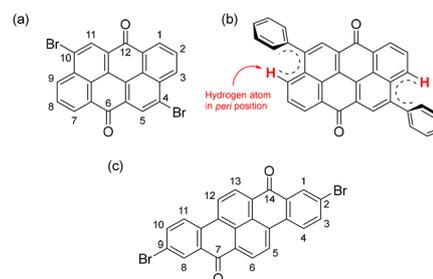
Fig. 1 Position numbering (a) and representation of the effect of the presence of a hydrogen atom in *peri* positions (in red at the 3 and 9 positions) of the vat orange 3 (b). Position numbering of vat orange 1 (c).

Paper

Materials Advances

synthesized, achieving power conversion efficiencies (PCE) of up to 1.2% in organic solar cells (OSCs) and charge carrier mobilities of up to 3.6 cm^2 V^{-1} s^{-1} in organic field-effect transistors (OFETs).

Herein, we report the synthesis, characterization and device performances of non-fullerene acceptors (NFAs) with vat orange 1 as a donor moiety in an acceptor–donor–acceptor (A–D–A) architecture. We hypothesized the addition of electron-withdrawing groups on each side of the dibenzo[b,def]chrysene donor core would lead to molecules with high molar extinction coefficient in the visible range. As electron-withdrawing groups, we selected three units that proved to be efficient for the preparation of NFAs, namely malononitrile, 2-(3-oxo-2,3-dihydroinden-1-ylidene)malononitrile (INCN) and 3-ethylrhodanine. The primary objective of this study is to explore the possibility of using low-cost, readily accessible **VO1** as a π-conjugated donating unit in a A–D–A architectures for photovoltaic application.

Results and discussion

To begin this study, we targeted simple structures such as compound **4** (Scheme 1). To ensure solubility of the materials, **VO1** was subject to reductive bis-*O*-alkylation with branched alkyl chains resulting in compound **1**.[12] Then, a two-fold Miyaura borylation to obtain compound **2** was performed, followed by a Suzuki–Miyaura cross-coupling reaction with 5-bromothiophene-2-carbaldehyde. Finally, compound **3** was engaged in a Knoevenagel condensation with malononitrile

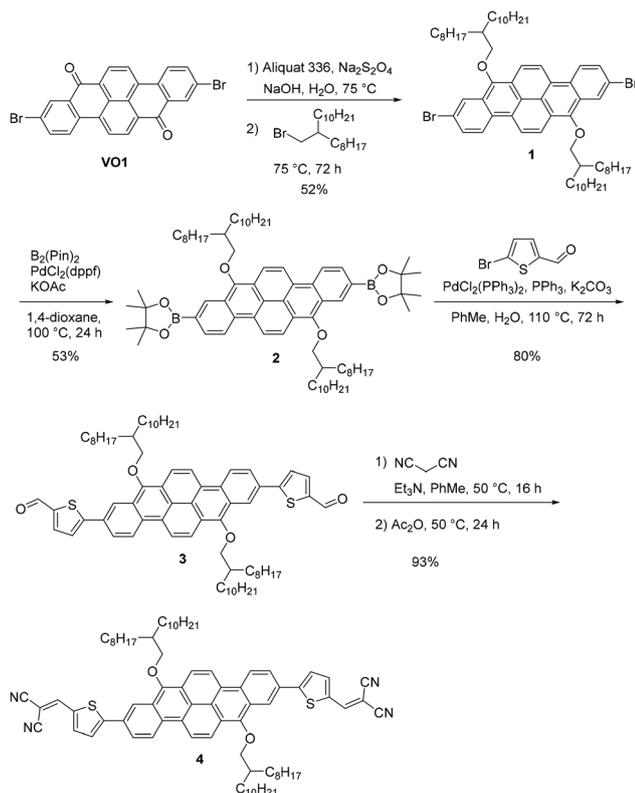Scheme 1 Synthesis of compound **4**.

using triethylamine as the base and acetic anhydride as the dehydrating reagent to provide compound **4** in excellent yield.

Unfortunately, compound **4** exhibits very low solubility in common organic solvents, making the synthesis of the intended INCN and 3-ethylrhodanine derivatives futile. Nonetheless, compounds **3** and **4** were characterized using UV-visible spectroscopy (Fig. S19) and cyclic voltammetry (Fig. S24 and S25) to assess the ability of electron-withdrawing groups on the dibenzo[b,def]chrysene core to modulate the optoelectronic properties. Interestingly, the addition of malononitrile moieties at both the 2 and 9 position of the dibenzo[b,def]chrysene unit results in a bathochromic shift of 73 nm in solution (389 *vs.* 462 nm) and a decrease of 0.3 eV in the band gap value. Also, a shoulder around 560 nm, which can be assigned to charge transfer, appeared upon the addition of the dicyanovinylene position of the dibenzo[b,def]chrysene unit.

The poor solubility of compound **4** is quite surprising, considering that the branched alkyl chain proved to be highly efficient at providing solubility in high molecular weight conjugated polymers.[21] We hypothesize that aggregation, driven by the strong π interactions of the dibenzo[b,def]chrysene core, might be responsible for this low solubility.

To improve the solubility and increase even further the donor character of the **VO1** core, the branched alkoxy chains were replaced with alkoxylated diphenylamine (DPA) moieties at the 7 and 14 positions. Moreover, the DPA moieties, lying perpendicular to the **VO1** core, are expected to generate enough steric hindrance to prevent π-stacking, thus improving the solubility of the final molecules.[22]

The synthesis of compounds **5** to **11** is presented in Scheme 2. First, a reductive amination of **VO1** with 4-octyloxy-aniline was performed to obtain compound **5** in 65% yield. In order to avoid solubility issues with the thiophene directly attached to the core like with compound **4**, it has been decided to use acetylene π-spacer to increase the degree of freedom of the end groups.[23,24] We found that **VO1** derivatives bearing thiophene units directly at the 2- and 9-positions, without a spacer, are generally insoluble as a result of strong intermolecular interactions. Thus, compound **5** was engaged in a two-fold Castro–Stephen–Sonogashira reaction with (triisopropylsilyl)acetylene (TIPSA) resulting in compound **6**. A two-fold Buchwald–Hartwig reaction with 1-bromo-4-(octyloxy)benzene provided compound **7** in 78% yield. The later was treated with tetrabutylammonium fluoride (TBAF) to deprotect the alkyne and a two-fold Castro–Stephen–Sonogashira reaction with 5-iodo-thiophene-2-carbaldehyde was performed to yield compound **8**. Finally, the A–D–A targeted compounds **9–11** were obtained from compound **8** using Knoevenagel condensation with the corresponding electron-withdrawing moiety. It is worth noting that the reaction conditions had to be optimized for every electron-acceptor used in this study and that no universal method applied to all of them. Malononitrile and 3-ethylrhodanine reacted well with compound **8** when amine base was used whereas INCN did not. In this case, only the Lewis acid-catalyzed reaction yielded the desired compound.[25] Unlike compound **4**, the resulting products **9–11** are highly soluble in common organic solvents.
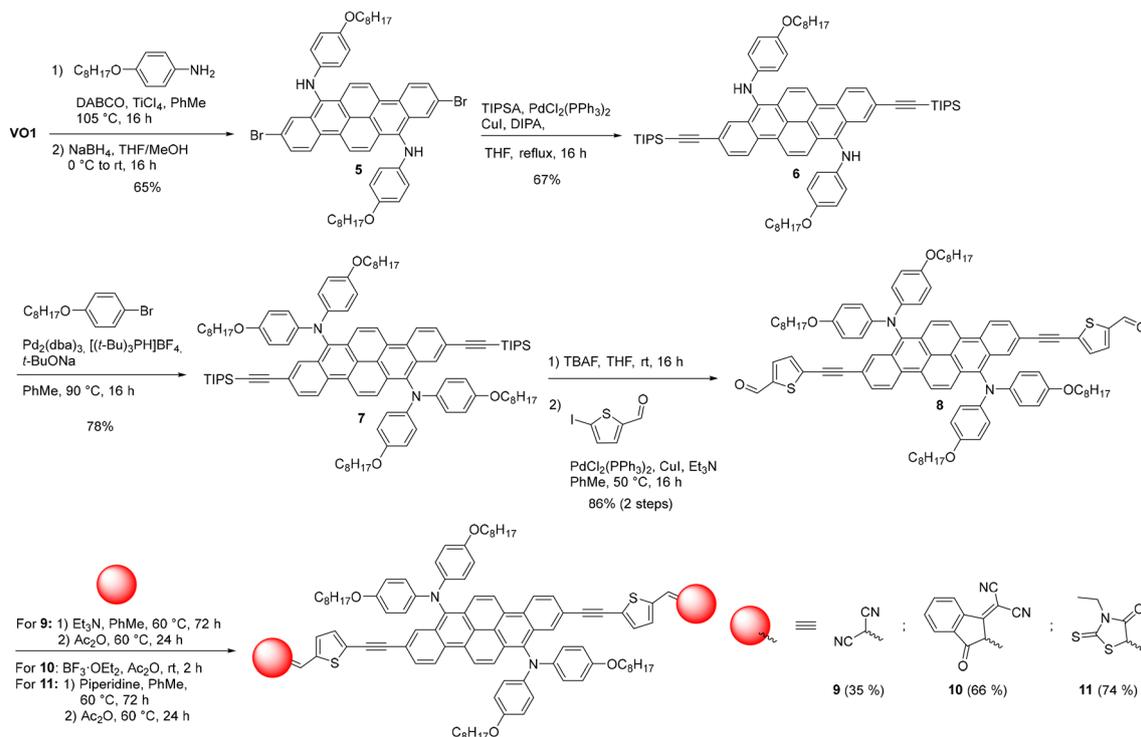
Scheme 2 Synthesis of compounds **9–11**.

Compounds **8–11** have been characterized using UV-visible spectroscopy in both solution and thin film (see Fig. S20–S23). As expected, the introduction of electron-withdrawing moieties at both ends of the molecules, as the result of a Knoevenagel condensation (compounds **9–11**), generates a bathochromic shift of the absorption peak (λ_{max}) between 80 and 166 nm both in solution and in thin film. Also, no significant change in the spectrum onsets (λ_{onset}) was observed except for compound **10** with its long tailing (see Fig. 2). Unexpectedly, the replacement of alkoxy moieties by DPA at the 7 and 14 positions did not yield to a significant decrease of the band gap values, likely due to the relatively high dihedral angle between the **VO1** core and the DPA units.
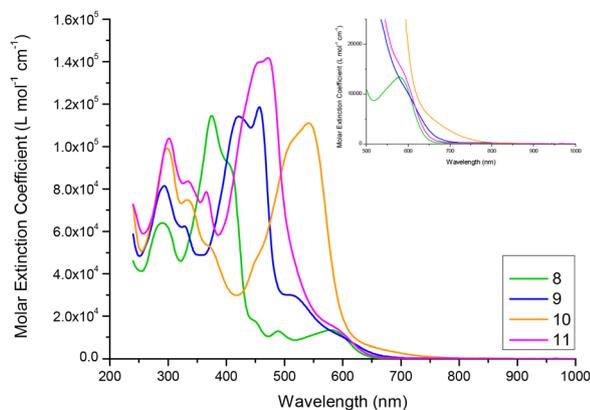
Fig. 2 UV-Vis molar extinction spectra of compounds **8–11** in chloroform solution.

The energy values of the highest occupied molecular orbitals (HOMO) and lowest unoccupied molecular orbitals (LUMO) of compounds **3–4** and **8–11** were measured using cyclic voltammetry (CV) and differential pulse voltammetry (DPV) (Table 1 and Table S3). As expected, the HOMO energy levels of the DPA derivatives (**8–11**) are higher than the alkoxy derivatives (**3**), whereas the LUMO energy levels of compounds **9–11** are lower in energy than for compound **8**. These results indicate an efficient electronic delocalization between the **VO1** core and the electron-withdrawing and groups at the 2 and 9 positions, resulting in a smaller band gap.

The thermal properties of compounds **8–11** were determined through thermogravimetric analysis (TGA) and differential scanning calorimetry (DSC) to assess their stability. TGA curves (Fig. S31) show that compound **8** was the most thermally stable with a 5% weight loss between 420 and 424 °C. The addition of electron-withdrawing units on the **VO1** core results in less stable materials which are decomposing faster than their precursor. It is especially the case for compounds **9** and **11** with an early decomposition at around 200 °C. Beside, it seems that all the molecules undergo a similar decomposition process with a significant weight loss between 400 and 480 °C. Considering that the weight loss was less significant for compounds **9–10** compared to **8**, this main decomposition can be attributed to the degradation of the DPA units due to their smaller contribution to the materials molecular weight. For compound **11**, the 3-ethylrhodanine seems to be way less stable than DPA.

To avoid decomposition during the DSC measurements, the samples were heated up to 160 °C for all molecules (Fig. S32–S35). The DSC results did not show any well-defined

Table 1 Optoelectronic properties of compounds **3–4** and **8–11**

Compound	$\lambda_{max}^{solution}$ (nm)	$\varepsilon_{max}^{solution}$ (10^4 L mol^{-1} cm^{-1})	$\lambda_{onset}^{solution\ a}$ (nm)	$E_g^{opt.,solution\ b}$ (eV)	E_{HOMO} (eV)	E_{LUMO} (eV)	$E_g^{elec\ c}$ (eV)
3	389	150	545	2.28	−5.20	−3.24	1.96
4	462	138	627	1.98	−4.86	−3.20	1.67
8	375	11.5	641	1.93	−5.01	−3.06	1.94
9	457	11.9	667	1.86	−5.00	−3.26	1.74
10	541	11.1	728	1.70	−4.99	−3.73	1.26
11	471	14.2	648	1.91	−4.99	−3.28	1.71

Optical measurements obtain in chloroform solution. [a] Determined using tangential curves with R^2 values over 0.93. [b] $E_g = 1240 \div \lambda_{onset}$. [c] $E_g^{elec} = E_{LUMO} - E_{HOMO}$, measurements made in dichloromethane solution with 0.1 M [n-Bu$_4$N][PF$_6$] as the supporting electrolyte using platinum wires as working and counter electrodes. The ferrocene peak was adjusted to 0.475 V versus Ag/Ag$^+$.[28] The ferrocene/ferrocenium couple was established at 4.8 V below the vacuum level.[29]

Table 2 OSC mean results for the devices made from compounds **8–11** with P3HT[a]

Compound as NFA	OSC architecture	J_{SC} (mA cm^{-2})	V_{OC} (V)	FF (%)	PCE (%)
8	Direct[b]	0.97	1.20	21	0.26
	Inverted[c]	1.36	0.77	45	0.46
9	Direct	0.15	0.90	20	0.03
	Inverted	0.32	0.53	39	0.07
10	Direct	0.11	0.63	30	0.02
	Inverted	0.14	0.59	31	0.03
11	Direct	0.54	0.80	30	0.15
	Invered	0.76	0.65	43	0.21

[a] The resulting devices had an active area of 10.5 mm^2 and were measured under AM 1.5G spectrum in a nitrogen-filled glovebox. [b] ITO/PEDOT:PSS/BHJ(1:1)/Ca/Al. [c] ITO/ZnO/BHJ(1:1)/MoO$_3$/Ag.

Table 3 OSC mean results for the devices made from compounds **8–11** with PC$_{61}$BM[a]

Compound as donor	OSC architecture	J_{SC} (mA cm^{-2})	V_{OC} (V)	FF (%)	PCE (%)
8	Direct[b]	0.65	0.76	29	0.14
	Inverse[c]	0.66	0.65	33	0.14
9	Direct	0.89	0.75	26	0.17
	Inverse	1.08	0.72	30	0.23
10	Direct	0.59	0.70	28	0.12
	Inverse	0.76	0.65	29	0.14
11	Direct	0.81	0.75	28	0.17
	Inverse	0.80	0.18	27	0.04

[a] The resulting devices had an active area of 10.5 mm^2 and were measured under AM 1.5G spectrum in a nitrogen-filled glovebox. [b] ITO/PEDOT:PSS/BHJ(1:1)/Ca/Al. [c] ITO/ZnO/BHJ(1:1)/MoO$_3$/Ag.

crystallization (T_c), melting (T_m) or glass transition (T_g) peaks in the range of 25 to 160 °C. This aligns with literature reports indicating that **VO1** and **VO3** derivatives containing alkynes or diphenylamines typically exhibit a T_c value around 300 °C.[17,20,26,27] This amorphous morphology might explain the difficulty we faced at growing crystals of these molecules.

Organic solar cells (OSCs)

Following the optoelectronic characterization of compounds **8–11**, we tested them as both electron acceptor and electron donor. Poly(3-hexylthiophene) (P3HT) has been selected to be the donor material when compounds **8–11** were used as acceptors, and [6,6]-phenyl-C$_{61}$-butyric acid methyl ester (PC$_{61}$BM) has been used as the acceptor material when compounds **8–11** were used as donor materials. Compounds **8–11** were mixed

with their counterpart in a 1:1 weight ratio without any additive in chlorobenzene at 90 °C in order to formulate bulk heterojunction (BHJ) solutions. Then, the solutions were spin-coated in order to prepare OSCs in two different architectures: direct (ITO/PEDOT:PSS/BHJ/Ca/Al) and inverted (ITO/ZnO/BHJ/MoO$_3$/Ag). Device fabrication and characterization procedures are detailed in the SI section.

The resulting devices were tested under AM 1.5G solar simulator in inert atmosphere in order to acquire the current density–voltage (J–V) curves. Regardless of the role of compounds **8–11** (donor or acceptor), the power conversion efficiency (PCE, %), fill factor (FF, %) and short-circuit current density (J_{SC}, A cm^{-2}) values were lower in direct architecture than the inverted one whereas the open-circuit voltage (V_{OC}, V) was higher (see Tables 2, 3 and Tables S12–S15). The only

exception to those trends was compound **11**, end-capped with 3-ethylrhodanine and mixed with $PC_{61}BM$ that exhibited a PCE value which is four times smaller in inverted architecture compared to the direct. This can be attributed to the small shunt resistance (R_{sh}, Ω), generating a significant current loss observed with the curves acquired in the dark.

The most efficient acceptor (paired with P3HT) was compound **8**, having the aldehydes, with a PCE of 0.46% in inverted architecture. This result is unexpected considering that compound **8** is the derivative with the weaker electron-withdrawing ability (see Fig. S30). This result could be rationalized by looking at the extinction curves of compound **8** and P3HT (presented in Fig. S75), which are the most complementary. The external quantum efficiency (EQE) curves of this combination (P3HT:**8**) result in the broadest and the highest values compared to the other combinations. This analysis can also be pushed further by looking at the energy levels of compounds **8–11** and P3HT (Fig. S30). In the case of compounds **9** and **11**, their frontier orbitals align with those of P3HT to act as n-type materials (with a lower LUMO energy level). For compound **10**, the LUMO is too deep compared to the P3HT one, which may result in less efficient exciton dissociation. Regarding compound **8**, its frontier orbitals (HOMO and LUMO) are higher in energy than P3HT ones (see Fig. S30), which would make the P3HT act as a n-type material. As suggested by Fahlman and co-workers,[30] significant vacuum level shifts may occur at D–A interfaces. This implies that HOMO and LUMO levels determined independently by CV measurements could be under- or overestimated relative to their actual values at the interface. Further investigations will be carried out on the P3HT:compound **8** blend to gain a clearer understanding of the unusual results observed.

Regarding the performances of compounds **8–11** as p-type semiconductors when paired with n-type $PC_{61}BM$, compound **9**, which is end-capped with malononitrile, achieved the highest PCE with of 0.23%, in an inverted architecture/structure. It has been observed that the J–V curves distribution as a function of our compound was narrower in the case of the blends compound:$PC_{61}BM$ than the P3HT:compound ones (especially in direct configuration), meaning that the donor character of the **VO1** core is not influenced by the end groups when alkyne is used as a π-bridge between the **VO1** core and the acceptor units. Looking at the frontier orbitals, it seems clear why poor performances were obtained with the HOMO of compounds **8–11** and $PC_{61}BM$ being spread apart by 1 eV leading to a quasi-impossible exciton separation.

Computational chemistry

Theoretical calculations were conducted on the compounds **8–11** to assess the optimized molecular geometries, the frontier orbitals distribution and energy, and simulated UV-visible spectra. The calculations were performed with Gaussian 16[31] using 3 different methods (B3LYP, ωB97xD and HF/PBE0[32]) on 6-31+G(d,p) level. Compounds **8–11** were compared with their counterparts developed on the reversed axis, as shown in Fig. 3, to evaluate whether motifs **8′–11′** might serve as better NFA candidates.

As expected, DPA units form greater dihedral angles with the **VO1** core for compounds **8–11** than for compounds **8′–11′** (see Tables S5–S7 and Fig. S36, S37), regardless of the method used. However, if the lower energetic configuration of DPA form an angle of 70–75° in compounds **8–11**, it may indicate that DPAs were not free to rotate and were fixed in a specific configuration, meaning that there is a greater energy barrier for the rotation of the DPA units on the 7 and 14 positions axis, whereas compounds **8′–11′** possess lower energetic configuration angles of 15–35°. Regarding the use of alkynes, calculations showed really small dihedral angles (0–5°) between the **VO1** core and the thiophene unit, except for compounds **8′–11′** with ωB97xD (25–40°).

Energy level calculations exhibit the same trend, regardless of the method used and the **VO1** orientation. Nonetheless, the introduction of malononitrile (**9** and **9′**) was the most effective to lower the HOMO in front of INCN (**10** and **10′**) and 3-ethylrhodanine (**11** and **11′**), using the aldehyde derivatives (**8** and **8′**) as the reference (Table 4). For the lowest unoccupied molecular orbitals (LUMO), INCN was the most effective to lower it before malononitrile and 3-ethylrhodanine. Looking at the calculated values, ωB97xD seems to overestimate how deep were the HOMO levels and to underestimate the LUMO values whereas B3LYP (Fig. 4) and HF/PBE0 were quite accurate. For the orbital distribution (HOMO–LUMO) on a compound, it was not significantly different between methods. Aldehyde derivatives exhibit a strong overlap between the HOMO and LUMO on the **VO1** core. For compounds **9–11** and **9′–11′**, the HOMO and LUMO orbitals are more localized on the DPA and on the electron-withdrawing units, respectively, especially for compounds **9–11**, resulting in a weaker frontier orbitals overlap (see Fig. S44–S67).

Looking at the calculated UV-visible spectra (time-dependent DFT, see Fig. S41–S43), we observed that compounds **8′–11′** have smaller optical band gap compared to **8–11**. Each method presents the same trend where compounds **8′–11′** oscillators were weaker and at lower energies compared
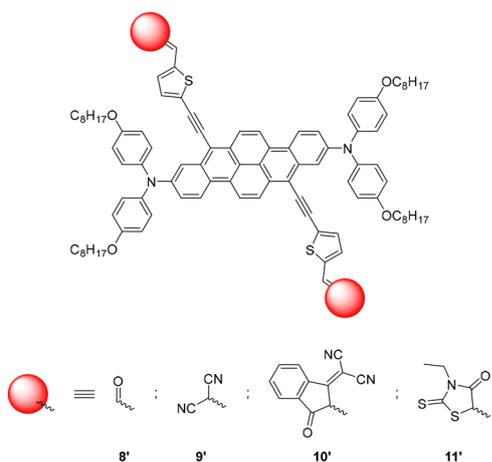

Fig. 3 Chemical structure of **8′–11′**.

Table 4 Frontier molecular orbital energy of compounds **8–11** and **8′–11′** based on calculation with B3LYP, ωB97xD or HF/PBE0 using 6-31+G(d,p) basis set in a PCM[a] solvation model in chloroform with a superfine integration grid

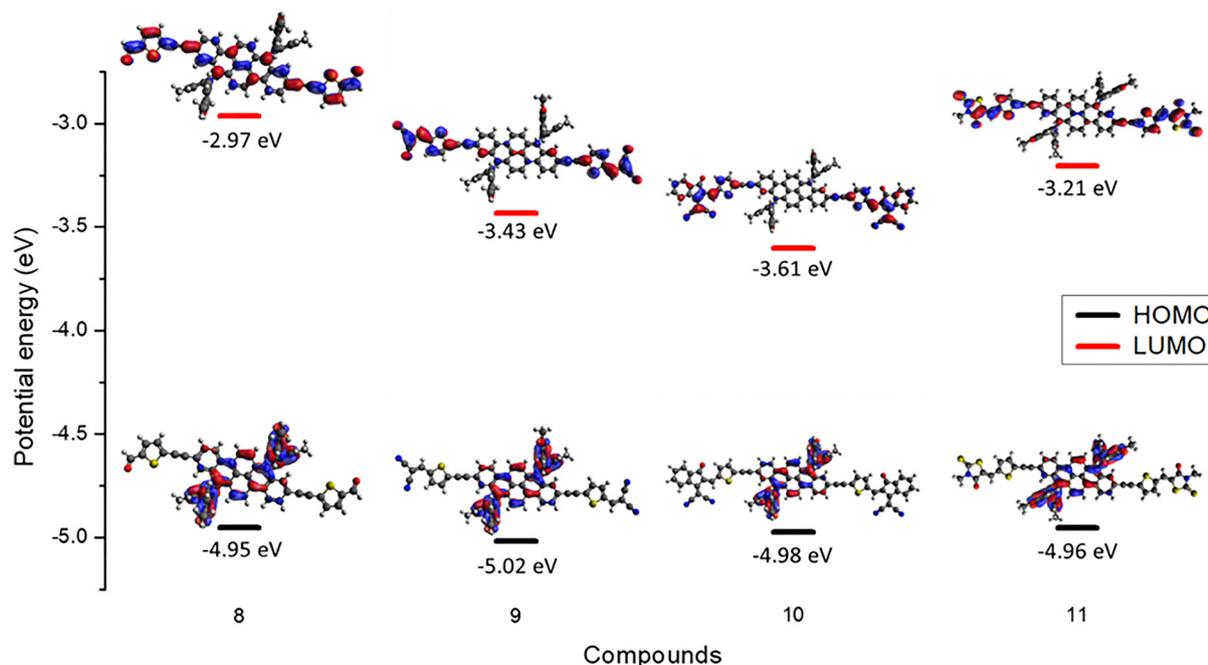| Method	B3LYP		ωB97xD		HF/PBE0	
Compound	HOMO (eV)	LUMO (eV)	HOMO (eV)	LUMO (eV)	HOMO (eV)	LUMO (eV)
8	−4.95	−2.97	−6.65	−1.34	−5.21	−2.70
9	−5.02	−3.43	−6.70	−1.79	−5.27	−3.13
10	−4.98	−3.61	−6.66	−2.00	−5.23	−3.31
11	−4.96	−3.21	−6.65	−1.59	−5.22	−2.93
8′	−4.98	−3.16	−6.64	−1.49	−5.26	−2.80
9′	−5.08	−3.56	−6.71	−1.85	−5.34	−3.20
10′	−5.05	−3.69	−6.61	−2.08	−5.28	−3.34
11′	−4.97	−3.33	−6.62	−1.74	−5.27	−2.99

[a] Polarizable continuum model.

Fig. 4 Kohn–Sham molecular orbitals of compounds **8–11** based on calculations at B3LYP/6-31+G(d,p) level using the PCM solvation model in chloroform with a superfine integration grid.

to **8–11**. Also, the INCN derivatives resulted in the more important bathochromic shift, followed by 3-ethylrhodanine and malononitrile. Furthermore, as observed experimentally, the onset value of compounds **8–11** is consistent. Finally, the B3LYP functional seems to underestimate the optical band gap with fewer vibrational details while HF/PBE0/HF overestimates it with well-defined vibronic transitions. Regarding TD-DFT calculations of **VO1** derivatives, the ωB97xD functional seems the most accurate.

Conclusions

Molecules derived from vat orange 1 in an A–D–A architecture were synthesized using diphenylamine moieties as solubilizing groups and tested in OSCs. These molecules exhibit a thermal stability up to 200 °C and no crystallisation behavior. The optical

band gap in solution and in thin films of those products ranged between 1.7 and 1.9 eV, and 1.6 and 1.8 eV, respectively. The derivatives were integrated into the active layer of organic solar cells yielding modest performances below 0.5% (PCE) as acceptor materials with P3HT and under 0.25% as donor materials with $PC_{61}BM$. Nonetheless, this study shows that compounds **8–11** can serve as both p- and n-type semiconductors. DFT calculations have been conducted with three methods (B3LYP, ωB97xD and HF/PBE0) and showed that the A–D–A architecture with the DPA units on the 7,14-axis of dibenzo[*b,def*]chrysene could be more promising than the 2,9-axis developed in this work. This conclusion sheds light on why **VO1** has been more extensively studied along this axis in the literature.[33,34] Further investigations are underway to determine whether n-type **VO1** semiconductor derivatives can be obtained by introducing electron-accepting groups closer to the core.

Author contributions

F. G. did the project conception, synthesis, optoelectronic and thermal characterization, device fabrication, computational chemistry, data analysis and writing – original draft. C. D. did supervision and writing – review & editing. E. P. did the synthesis. G. W. did the project administration, provided resources and writing – review & editing. J.-F. M. did the project conception and administration, funding acquisition and writing – original draft.

Conflicts of interest

There are no conflicts to declare.

Data availability

The data supporting this article have been included as part of the supplementary information (SI). Supplementary information: Experimental protocols, optoelectronic and thermal characterizations, computational chemistry and organic solar cells results. See DOI: https://doi.org/10.1039/d5ma00553a.

Acknowledgements

Notes and references

1 J. B. Giguère, Q. Verolet and J. F. Morin, *Chem. – Eur. J.*, 2013, **19**, 372–381.
2 Y. J. Kim, J. S. Lee, J. Hong, Y. Kim, S. B. Lee, S.-K. Kwon, Y.-H. Kim and C. E. Park, *J. Polym. Sci., Part A: Polym. Chem.*, 2016, **54**, 2559–2570.
3 Q. Liu, Y. Wang, L. Arunagiri, M. Khatib, S. Manzhos, K. Feron, S. E. Bottle, H. Haick, H. Yan and T. Michinobu, *Mater. Adv.*, 2020, **1**, 3428–3438.
4 M. Desroches and J.-F. Morin, *Macromol. Rapid Commun.*, 2018, **39**, 1800214.
5 C. Aumaitre, D. Fong, A. Adronov and J.-F. Morin, *Polym. Chem.*, 2019, **10**, 6440–6446.
6 K. Mulla and J. F. Morin, *ChemistrySelect*, 2023, **8**, e202300611.
7 L. Zhang, B. Walker, F. Liu, N. S. Colella, S. C. B. Mannsfeld, J. J. Watkins, T.-Q. Nguyen and A. L. Briseno, *J. Mater. Chem.*, 2012, **22**, 4266–4268.
8 M. Li, M. Xiao and Z. Li, *RSC Adv.*, 2021, **11**, 39625–39635.
9 B. Kahraman, C. Yumusak, F. Mayr, D. Wielend, K. Kotwica, C. V. Irimia, E. Leeb, M. Cobet, N. S. Sariciftci and M. Irimia-Vladu, *J. Mater. Chem. C*, 2024, **12**, 3838–3853.
10 F. Lirette, C. Aumaitre, C.-É. Fecteau, P. A. Johnson and J.-F. Morin, *ACS Omega*, 2019, **4**, 14742–14749.
11 A. Darvish, F. Lirette, I. Fernandez and J. F. Morin, *Chemistry*, 2025, **31**, e202403456.
12 F. Gagnon, V. Tremblay, A. Soldera, M. U. Ocheje, S. Rondeau-Gagné, M. Leclerc and J.-F. Morin, *Mater. Adv.*, 2022, **3**, 599–603.
13 D. A. Zherebtsov, V. V. Sharutin, S. A. Nayfert, M. A. Polozov, C. P. S. Dharan and K. Rajakumar, *Crystallogr. Rep.*, 2022, **67**, 371–375.
14 K. B. Burke, Y. Shu, P. Kemppinen, B. Singh, M. Bown, I. I. Liaw, R. M. Williamson, L. Thomsen, P. Dastoor, W. Belcher, C. Forsyth, K. N. Winzenberg and G. E. Collis, *Cryst. Growth Des.*, 2012, **12**, 725–731.
15 A. N. Simonov, P. Kemppinen, C. Pozo-Gonzalo, J. F. Boas, A. Bilic, A. D. Scully, A. Attia, A. Nafady, E. A. Mashkina, K. N. Winzenberg, S. E. Watkins and A. M. Bond, *J. Phys. Chem. B*, 2014, **118**, 6839–6849.
16 F. H. Scholes, T. Ehlig, M. James, K. H. Lee, N. Duffy, A. D. Scully, T. B. Singh, K. N. Winzenberg, P. Kemppinen and S. E. Watkins, *Adv. Funct. Mater.*, 2013, **23**, 5655–5662.
17 K. N. Winzenberg, P. Kemppinen, G. Fanchini, M. Bown, G. E. Collis, C. M. Forsyth, K. Hegedus, T. B. Singh and S. E. Watkins, *Chem. Mater.*, 2009, **21**, 5701–5703.
18 D. Gruszecki, B. Singh, M. Bown and D. Lewis, *J. Phys. D: Appl. Phys.*, 2012, **45**, 045104.
19 L. Zhang, A. Fonari, Y. Zhang, G. Zhao, V. Coropceanu, W. Hu, S. Parkin, J.-L. Brédas and A. L. Briseno, *Chem. – Eur. J.*, 2013, **19**, 17907–17916.
20 L. A. Stevens, K. P. Goetz, A. Fonari, Y. Shu, R. M. Williamson, J.-L. Brédas, V. Coropceanu, O. D. Jurchescu and G. E. Collis, *Chem. Mater.*, 2015, **27**, 112–118.
21 A. Darvish, M. Mooney, T. C. Gomes, F. Gagnon, S. Rondeau-Gagné and J.-F. Morin, *J. Mater. Chem. C*, 2025, **13**, 5241–5247.
22 M. Desroches and J.-F. Morin, *Chem. – Eur. J.*, 2018, **24**, 2858–2862.
23 R. Mishra, R. Regar, V. Singh, P. Panini, R. Singhal, M. L. Keshtov, G. D. Sharma and J. Sankar, *J. Mater. Chem. A*, 2018, **6**, 574–582.
24 J.-B. Giguère, J. Boismenu-Lavoie and J.-F. Morin, *J. Org. Chem.*, 2014, **79**, 2404–2418.
25 H. Fu, J. Yao, M. Zhang, L. Xue, Q. Zhou, S. Li, M. Lei, L. Meng, Z.-G. Zhang and Y. Li, *Nat. Commun.*, 2022, **13**, 3687.
26 Y. Shu, G. E. Collis, C. J. Dunn, P. Kemppinen, K. N. Winzenberg, R. M. Williamson, A. Bilic, T. B. Singh, M. Bown, C. R. McNeill and L. Thomsen, *J. Mater. Chem. C*, 2013, **1**, 6299–6307.
27 H. D. Pham, K. Hayasake, J. Kim, T. T. Do, H. Matsui, S. Manzhos, K. Feron, S. Tokito, T. Watson, W. C. Tsoi, N. Motta, J. R. Durrant, S. M. Jain and P. Sonar, *J. Mater. Chem. C*, 2018, **6**, 3699–3708.
28 J. R. Aranzaes, M.-C. Daniel and D. Astruc, *Can. J. Chem.*, 2006, **84**, 288–299.
29 J. Pommerehne, H. Vestweber, W. Guss, R. F. Mahrt, H. Bässler, M. Porsch and J. Daub, *Adv. Mater.*, 2004, **7**, 551–554.

30 X. e Li, Q. Zhang, J. Yu, Y. Xu, R. Zhang, C. Wang, H. Zhang, S. Fabiano, X. Liu, J. Hou, F. Gao and M. Fahlman, *Nat. Commun.*, 2022, **13**, 2046.

31 M. J. Frisch, G. W. Trucks, H. B. Schlegel, G. E. Scuseria, M. A. Robb, J. R. Cheeseman, G. Scalmani, V. Barone, G. A. Petersson, H. Nakatsuji, X. Li, M. Caricato, A. V. Marenich, J. Bloino, B. G. Janesko, R. Gomperts, B. Mennucci, H. P. Hratchian, J. V. Ortiz, A. F. Izmaylov, J. L. Sonnenberg, D. Williams-Young, F. Ding, F. Lipparini, F. Egidi, J. Goings, B. Peng, A. Petrone, T. Henderson, D. Ranasinghe, V. G. Zakrzewski, J. Gao, N. Rega, G. Zheng, W. Liang, M. Hada, M. Ehara, K. Toyota, R. Fukuda, J. Hasegawa, M. Ishida, T. Nakajima, Y. Honda, O. Kitao, H. Nakai, T. Vreven, K. Throssell, J. A. Montgomery Jr., J. E. Peralta, F. Ogliaro, M. J. Bearpark, J. J. Heyd, E. N. Brothers, K. N. Kudin, V. N. Staroverov, T. A. Keith, R. Kobayashi, J. Normand, K. Raghavachari, A. P. Rendell, J. C. Burant, S. S. Iyengar, J. Tomasi, M. Cossi, J. M. Millam, M. Klene, C. Adamo, R. Cammi, J. W. Ochterski, R. L. Martin, K. Morokuma, O. Farkas, J. B. Foresman and D. J. Fox, 2016.

32 M. Mainville, R. Ambrose, D. Fillion, I. G. Hill, M. Leclerc and P. A. Johnson, *ACS Appl. Energy Mater.*, 2021, **4**, 11090–11100.

33 N. Dardenne, R. Cardia, J. Li, G. Malloci, G. Cappellini, X. Blase, J.-C. Charlier and G.-M. Rignanese, *J. Phys. Chem. C*, 2017, **121**, 24480–24488.

34 Y. Kim, S. B. Lee, S. H. Jang, T. K. An, S. H. Kim, Y.-H. Kim and C. E. Park, *Dyes Pigm.*, 2016, **130**, 176–182.